Effects of the insulated magnetic field and oblique incidence of electrons on the multipactor in MILO*

Fan Jie-Qing(范杰清)† and Hao Jian-Hong(郝建红)

College of Electric and Electronic Engineering, North China Electric Power University, Beijing 102206, *China*

(Received 30 November 2009; revised manuscript received 26 November 2010)

The theoretical analysis and actual performance of the single-surface multipactor discharge model in the presence of a magnetic field are conducted through simulations. The effects of the magnitude of the insulated magnetic field and the oblique incidence of electrons on the multipactor are analysed. The results show that the multipactor susceptibility region shrinks gradually as the magnetic field increases when the electron cyclotron frequency is close to the RF frequency of the electric field. As a result, the evolution of the multipactor discharge will reach saturation earlier and become saturated at a higher level than the case when the magnetic field is absent, but the change of evolution and saturation as the insulated magnetic field increases is not obvious.

Keywords: multipactor, susceptibility diagram, insulated magnetic field

PACS: 84.40.Fe, 52.20.Fs, 52.40.Db **DOI:** 10.1088/1674-1056/20/6/068402

1. Introduction

The multipactor discharge is an avalanche caused by secondary electron emission from the device walls. The multipactor phenomenon can be observed in a wide range of frequency (from MHz to GHz) in various microwave systems,[1−5] e.g., high-power microwave (HPM) sources, accelerators, the microwave system of satellites or missiles, antenna systems and communication system.The multipactor can lead to the emergence of large amount of plasmas, wall surface heating, noise level increasing, breakdown or destructive damage in the device.

An important characteristic of pulse shortening is that it limits the energy enhancement of a microwave pulse, which is the main obstacle that hinders HPMs from practical applications. Many researchers have showed[1,4,6] that the gas breakdown time caused by a multipactor is much shorter than the electron-beam instability time or the plasma expansion time of the cathode and collector at a gigawatt power level. Consequently, the issues of pulse shortening and HPM source device capability enhancement have attracted much attention over the last decade.

The magnetic field is, in general, ignored in the multipactor calculation. This approximation is only valid when electrons with a first crossing energy are considered.[6] However, when the electron energy is powerful enough, the electron cyclotron motion caused by the insulated magnetic field is important for accumulating cyclotron energy and thus influences the characteristics of the cyclotron. Practically, since the insulated magnetic field and DC electric field unusually act on the same plane, it is necessary to consider the effects of the magnitude of the insulated magnetic field even though the electron velocity is relatively low. The insulated magnetic field plays an important role,[1] especially at the initial stage of multipactor discharge when the surface positive charge density and DC electric field are very low. In this paper, the effects of the magnitude of the insulated magnetic field on the multipactor are analysed in detail based on the work of Ref. [7].

2. The dynamic equation of a single-surface multipactor

Figure 1 shows the schematic of a single-surface multipactor discharge. In general, in the wave-beam

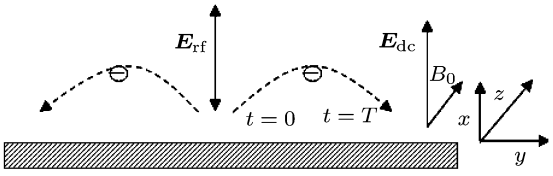


Fig. 1. Schematic diagram of a single-surface multipactor process.

*Project supported by the High Power Radiation Key Laboratory Foundation of the National High Technology Research and Development Program of China (Grant No. 20050601).

†Corresponding author. E-mail: fanjieqing@ncepu.edu.cn

© 2011 Chinese Physical Society and IOP Publishing Ltd

interaction region of a magnetically insulated line oscillator (MILO), there is a relativity electron beam, a insulated magnetic field $\boldsymbol{B}_0$ provided by the internal current of the tube, an RF electric field $\boldsymbol{E}_{\rm rf} = \boldsymbol{E}_{\rm rf0}\sin(\omega t+\theta_0)$ which is normal to the surface (in x direction), and a static electric field caused by space charge (including secondary electrons accumulation). According to Refs. [7] and [8], the dynamic equations for secondary electrons emitted from the surface are

$$m\frac{{\rm d}^2x}{{\rm d}t^2} + m\Omega^2 x = e\,|E_{\rm dc}(x)| - eE_{\rm rf0}\sin(\omega t+\theta_0), \quad (1)$$

$$\frac{{\rm d}y}{{\rm d}t} = \Omega x, \quad (2)$$

$$\Omega = \frac{eB_0}{mc}, \quad (3)$$

where Ω is the electron cyclotron frequency in a magnetic field (B_0). Because the loss of magnetical insulation appears somewhere in the MILO, the magnetic field was neglected in order to look into the basic physical characteristics of the multipactor in the past work. However, the magnetic field becomes important for single-surface multipactor discharge in many cases, especially when the DC electric field is weak. When both the insulated magnetic field and the space charge are considered, we can assume that B_0 varies slowly and thus can be taken out of the integral of Eq. (1) under a typical condition of $\Omega < \omega$. The electron displacement and velocity equations are obtained under the initial conditions[8]

$$x = C_1\cos\Omega t + C_2\sin\Omega t + \frac{\omega v_{\rm rf_0}}{(\omega^2-\Omega^2)}\sin(\omega t+\theta_0) + \frac{v_{\rm dc}}{\Omega}, \quad (\Omega\neq\omega), \quad (4)$$

$$\frac{{\rm d}x}{{\rm d}t} = -C_1\Omega\sin\Omega t + C_2\Omega\cos\Omega t + \frac{\omega^2 v_{\rm rf_0}}{\omega^2-\Omega^2}\cos(\omega t+\theta_0), \quad (\Omega\neq\omega), \quad (5)$$

$$C_1 = -\frac{\omega v_{\rm rf_0}}{\omega^2-\Omega^2}\sin\theta_0 - \frac{v_{\rm dc}}{\Omega}, \quad (6)$$

$$C_2 = \frac{v_{0x}}{\Omega} - \frac{\omega^2 v_{\rm rf_0}}{\Omega(\omega^2-\Omega^2)}\cos\theta_0, \quad (7)$$

where $v_{\rm rf_0} = eE_{\rm rf_0}/m\omega$, $v_{\rm dc} = eE_{\rm dc}/m\Omega = E_{\rm dc}/B_0c$, θ_0 is the initial RF phase, and v_{0x} is electron initial velocity in x direction.

The secondary electron emission yield (δ) is calculated by using Vaughan's empirical formula,[9,10]

$$\delta = \delta_{\rm m}[\varepsilon\,{\rm e}^{1-\varepsilon}]^g, \quad (8)$$

$$g = \begin{cases} 0.62, & \varepsilon \le 1, \\ 0.25, & \varepsilon > 1, \end{cases} \quad (9)$$

$$\varepsilon = \frac{E_{\rm i}-E_{\rm i0}}{E_{\rm m}-E_{\rm i0}}, \quad (10)$$

$$\delta_{\rm m} = \delta_{\rm m0}(1+k_{\rm s}\alpha_{\rm i}^2/2\pi), \quad (11)$$

$$E_{\rm m} = E_{\rm m0}(1+k_{\rm s}\alpha_{\rm i}^2/\pi), \quad (12)$$

where $\delta_{\rm m0}$ is the maximum secondary emission yield at normal incidence, $E_{\rm m0}$ is its corresponding impact energy, $E_{\rm i0}$ is the energy threshold for secondary electron emission, $k_{\rm s}$ is the smooth factor of the surface and $\alpha_{\rm i}$ is the incident angle of a primary electron.

3. Effects of the insulated magnetic field on multipactor discharge

In order to examine the basic physical characteristics about the dependence of multipactor discharge on the insulated magnetic field, we add the resonant condition $\omega t+\theta_0 = 2\pi$ and boundary condition $x = 0$ Eqs. (4) and (5), and thus obtain the resonant equation and impact velocity of the electron incidence on the wall surface as follows:

$$C_1\cos(2\pi k - k\theta_0) + C_2\sin(2\pi k - k\theta_0) + \frac{v_{\rm dc}}{\Omega} = 0, \quad (13)$$

$$v_{\rm i} = -C_1\Omega\sin(2\pi k - k\theta_0) + C_2\Omega\cos(2\pi k - k\theta_0) + \frac{1}{1-k^2}v_{\rm rf0}, \quad (14)$$

where, $k(=\Omega/\omega<1)$ is the ratio of cyclotron frequency to RF frequency. It characterizes the insulated magnetic field when the RF frequency is given. So the dependence of multipactor discharge on the insulated magnetic field can be described by k.

We now assume that the electron initial velocity is low and the condition of $v_0 \ll v_{\rm rf_0}$ is employed in Eq. (14). The impact velocity of the electron is derived as follows:

$$v_{\rm i} = \frac{v_{\rm rf_0}}{1-k^2}[k\sin\theta_0\sin(2\pi k - k\theta_0) - \cos\theta_0\cos(2\pi k - k\theta_0) + 1] + v_{\rm dc}\sin(2\pi k - k\theta_0). \quad (15)$$

Equation (13) is rewritten as

$$v_{\rm dc} = \frac{v_{\rm rf_0}}{(1-k^2)\,[1-\cos(2\pi k - k\theta_0)]} \times [k\sin\theta_0\cos(2\pi k - k\theta_0) + \cos\theta_0\sin(2\pi k - k\theta_0)]. \quad (16)$$

Substituting Eq. (16) into Eq. (15), we obtain

$$v_{\rm i} = g(k,\theta_0)v_{\rm rf_0}, \quad (17)$$

$$g(k,\theta_0) = \frac{1}{(1-k^2)}\Big\{[k\sin\theta_0\sin(2\pi k - k\theta_0) - \cos\theta_0\cos(2\pi k - k\theta_0) + 1] + \frac{\sin(2\pi k - k\theta_0)}{1-\cos(2\pi k - k\theta_0)} \times [k\sin\theta_0\cos(2\pi k - k\theta_0) + \cos\theta_0\sin(2\pi k - k\theta_0)]\Big\}. \quad (18)$$

Setting E_1 and E_2 to be the first and second crossed-over points, respectively, with $\delta = 1$. Multipactor discharge occurs only when the impact energy $E_{\rm i}$ lies between E_1 and E_2. Since $v_1 = \sqrt{2E_1/m}$, $v_2 = \sqrt{2E_2/m}$, the multipactor occurs only when $v_1 < v_{\rm i} < v_2$. Applying this condition to Eq. (17), we have

$$v_1 < g(k,\theta_0)v_{\rm rf_0} < v_2, \quad (19)$$

where $g(k,\theta_0)$ is a function of k and θ_0. Clearly, the multipactor susceptibility region and the $v_{\rm rf_0}$ range where the multipactor occurrs decrease as $g(k,\theta_0)$ increases when the values of v_1 and v_2 are given (see Fig. 2).

Figures 2(a) and 2(b) show that $g(k,\theta_0)$ is mainly affected by k when θ_0 is small, and by θ_0 when θ_0 is large. Therefore, when θ_0 is small, the resonant region, where the multipactor discharge is most serious, is more sensitive to k. When θ_0 is large, the effect of k on the multipactor weakens, and the effect of θ_0 becomes important. We observe that the "valley" values appear when $\theta_0 \approx 236^\circ$ in Fig. 2(b), which demonstrates that the multipactor discharge is enhanced.

The $g(k,3.6^\circ)$ increases monotonously as k increases (see Figs. 2(a) and 2(c)), and, as a result, the multipactor resonant and susceptibility region shrinks. However, figures 2(b) and 2(d) show that $g(k,\theta_0)$ decreases slightly but monotonously when θ_0 close near to 236°, leading to the expansion of multipactor resonant and susceptibility region.

Since the initial RF phase is different for different secondary electrons and different impacts, statistical results of N primary electrons are considered based on Monte Carlo methods. The energy of the emitted electrons is assigned randomly using the rectangular distribution,[7,11] and the RF phase θ_0 is assumed to be equally distributed from 0 to 2π by N samples. Then, we have

$$g(k) = \sqrt[N]{g_1(k,\theta_{01})g_2(k,\theta_{02})\ldots g_{\rm m}(k,\theta_{0m})}. \quad (20)$$

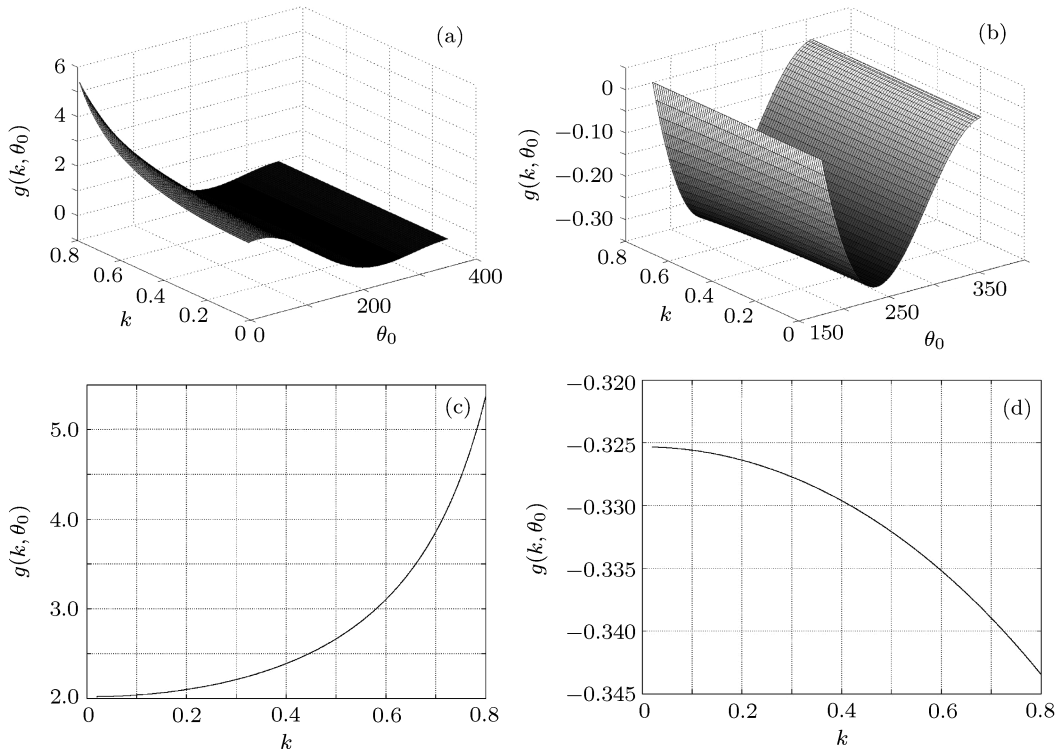


Fig. 2. Change of $g(k,\theta_0)$ as a function of k and θ_0 for (a) $\theta_0 \in [0,2\pi]$, (b) $\theta_0 \in [\pi,2\pi]$, (c) $\theta_0 = 36^\circ$, and (d) $\theta_0 = 236^\circ$. Panel (b) is a close-up view of panel (a).

Figure 3 shows that, when $0.02 < k < 0.8$, $g(k)$ in general increases as k increases, but with oscillations. We also note that $g(k)$ increases slowly when the insulated magnetic field (k) is weak, but $g(k)$ becomes more sensitive to k when $k > 0.5$. Therefore, the resonant and susceptibility region of the multipactor shrinks gradually as k increases, and such a dependence is not so evident when $k < 0.12$.

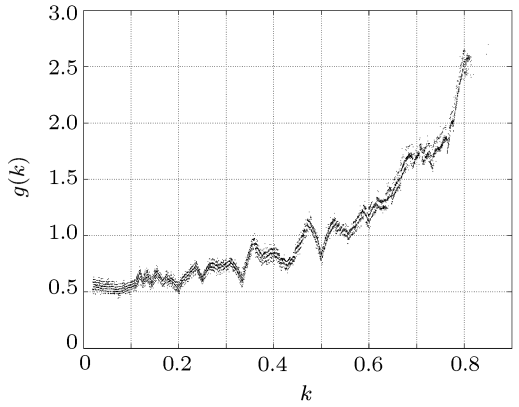


Fig. 3. The dependence of $g(k)$ on k.

4. Susceptibility diagram and multipactor temporal evolution

4.1. Effects of magnetic field on the susceptibility diagram and multipactor discharge evolution

4.1.1. Effect of the insulated magnetic field on the susceptibility diagram

Taking copper for example, the susceptibility diagrams for different cyclotron frequencies are plotted in Fig. 4, where the simulation parameters are $k_{\rm s} = 2.0$, $f = 2$ GHz, $\delta_{\rm m0} = 2.0$, $E_0 = 15$ eV, $E_{\rm m0} = 400$ eV, and $\alpha_{\rm i} = \pi/2$.

It can be shown that (i) the multipactor susceptibility region with $\delta > 1$ shifts as the insulated magnetic field (k) increases; (ii) figures 4(a)–4(d)

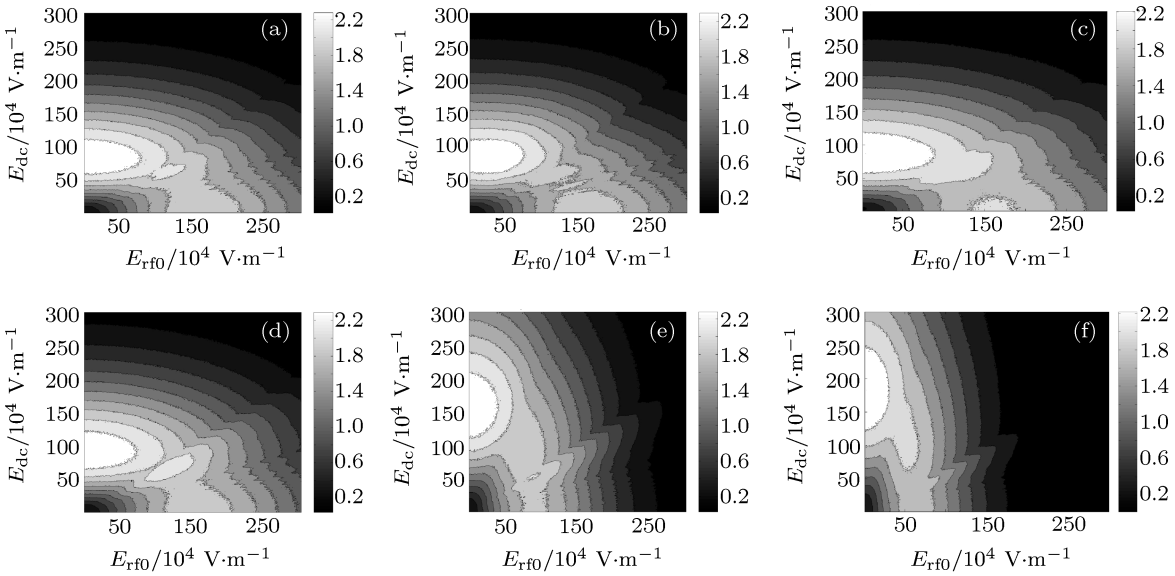


Fig. 4. The multipactor discharge susceptibility diagram for different k for (a) $k = 0.37$, (b) $k = 0.375$, (c) $k = 0.382$, (d) $k = 0.41$, (e) $k = 0.699$, and (f) $k = 0.8$.

show that the resonant region with maximum yield ($\delta \approx \delta_{\rm m0}$) shrinks slightly in local range of k, but the peak of the resonant region slightly increases when k approaches 0.38, which corresponds to the "valley" in Fig. 3. The results agree well with the analysis in Section 3; (iii) As k increases, the resonant region with maximum yield will emerge in the region where DC electric field is enhanced and the RF electric field is reduced. It can be explained that the electron impact velocity, magnetic field k, and the RF electric field must satisfy the relation of

$$v_{\rm i} \longrightarrow f[\sin(2k\pi - k\theta_0), \cos(2k\pi - k\theta_0)]\frac{v_{\rm rf0}}{1-k^2}$$

[see Eq. (15)], and that the multipactor must satisfy $v_1 < v_{\rm i} < v_2$ for the single-surface multipactor model. During the half RF period in which the DC electric field, magnetic field and the RF electric field are all in

the same direction, the force that pushes electrons to return to the wall surface is enhanced as k increases, and a weaker RF electric field is needed to ensure that the impact energy falls into $E_1 \sim E_2$.

4.1.2. Effects of the magnetic field on the temporal evolution of the multipactor

With the increasing number of secondary electrons, the normal DC electric field produced by the space charge becomes stronger, which accelerates electrons back to the surface. Therefore, the number of secondary electrons, the DC electric field and the insulated magnetic field are restricted reciprocally in the interacting region. Thus, the electron number of multipactor discharge will reach saturation (steady multipactor charge) when the restricting force reaches balance.

We now consider a one-dimensional case in which the electron beam is assumed to be thin sheets, the surface charge density is $\sigma_{\rm e} = -N_{\rm super}e/A$ (A is the surface area) and the ratio of real particles to superparticles is kept constant $N_{\rm super}$ for every simulation. According to the charge conservation law, the equivalent surface charge density $\sigma_{\rm eq}$ and the total number $N_{\rm e}$ of secondary electrons in the cavity must satisfy

$$\sigma_{\rm eq} + N_{\rm e}\sigma_{\rm e} = 0. \tag{21}$$

The normal electric field is obtained by $E_{_{\rm dc}} = \sigma_{\rm eq}/\varepsilon_0$ (we do not consider the external DC voltage, because it is a constant for all electrons), where ε_0 is the vacuum permittivity.

Using copper and taking $\delta_{\rm m0} = 2.0$, $E_{\rm m0} = 400$ eV, $E_{\rm i0} = 15$ eV, $k_{\rm s} = 2.0$, and $\alpha_{\rm i} = \pi/2$, the secondary electrons temporal evolution curves are plotted as shown in Fig. 5.

It can be shown: (i) Whether the insulated magnetic field is present or not, the number of electrons fluctuates around the saturation state. (ii) When the RF frequency ω and the amplitude $v_{\rm rf_0}$ are given, multipactor discharge reaches saturation earlier and saturates at a higher level than the case in which insulated magnetic field is absent. As k increases, the saturation level will be slightly higher, but it will take more time for the multipactor discharge to reach saturation. This phenomenon can be explained as follows: during the period of the electron flight, the insulated magnetic field pulls the electrons back to the wall surface, so the secondary electron emission yield will increase. In addition, the insulated magnetic field will shorten the electrons' fight transit time and the energy of electrons obtained from the RF field will decrease. Thus the electron impact energy deviates from the resonant energy range where the secondary electrons are emitted. They are mutual constraints. During the initial period of the evolution, the former dominates when k increases from zero. So the multipactor discharge occurs easier. However, the latter dominates gradually as k increases and the effect of $E_{\rm i}$ deviating from the multipactor resonant region exceeds the increase of δ, so it will take a more time for the multipactor to reach saturation.

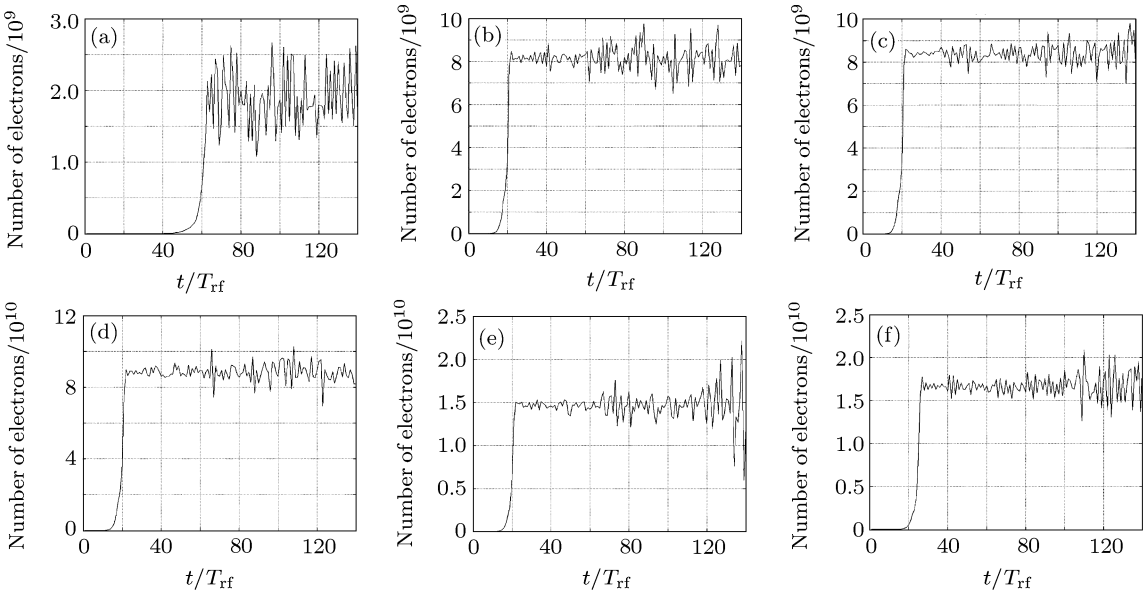


Fig. 5. The temporal evolution of secondary electrons for different k at $f = 2$ GHz and $E_{\rm rf_0} = 1.0$ MV/m for (a) no magnetic field effects, (b) $k = 0.375$, (c) $k = 0.382$, (d) $k = 0.41$, (e) $k = 0.699$, and (f) $k = 0.8$.

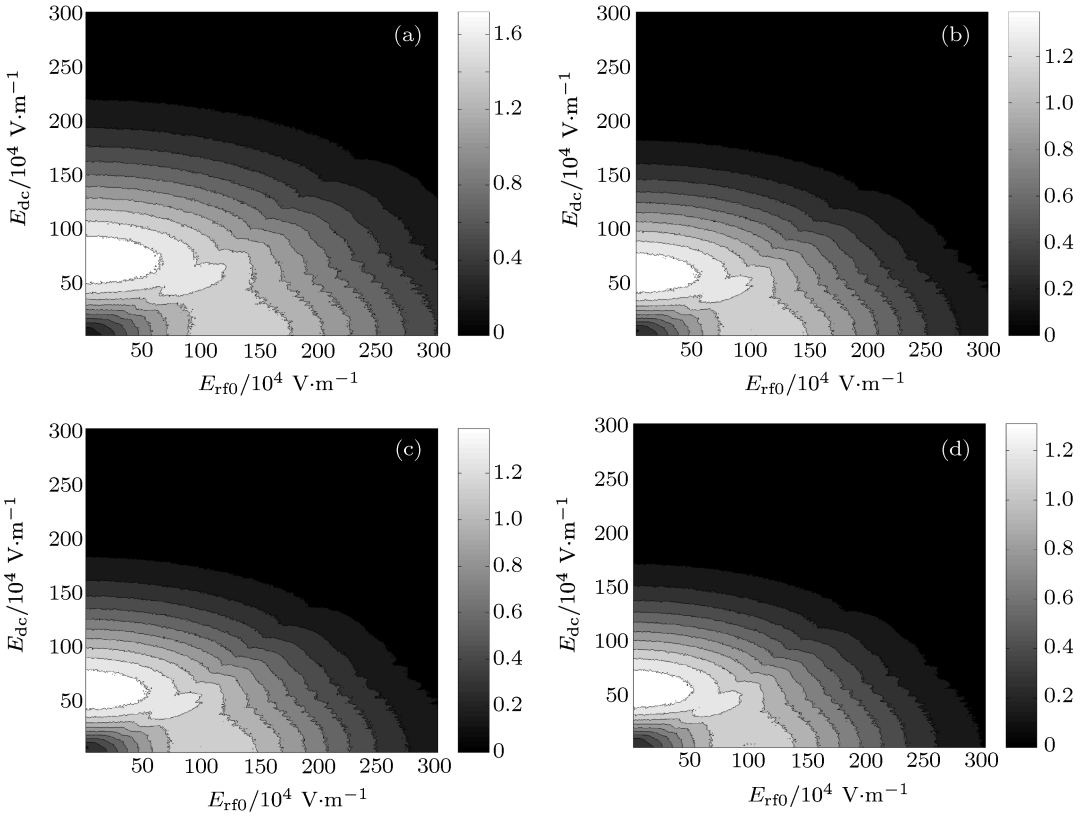


Fig. 6. The susceptibility diagram for different $\alpha_{\rm i}$ for (a) $\alpha_{\rm i} = 5\pi/12$, (b) $\alpha_{\rm i} = \pi/4$, (c) $\alpha_{\rm i} = \pi/6$, and (d) $\alpha_{\rm i} = \pi/12$.

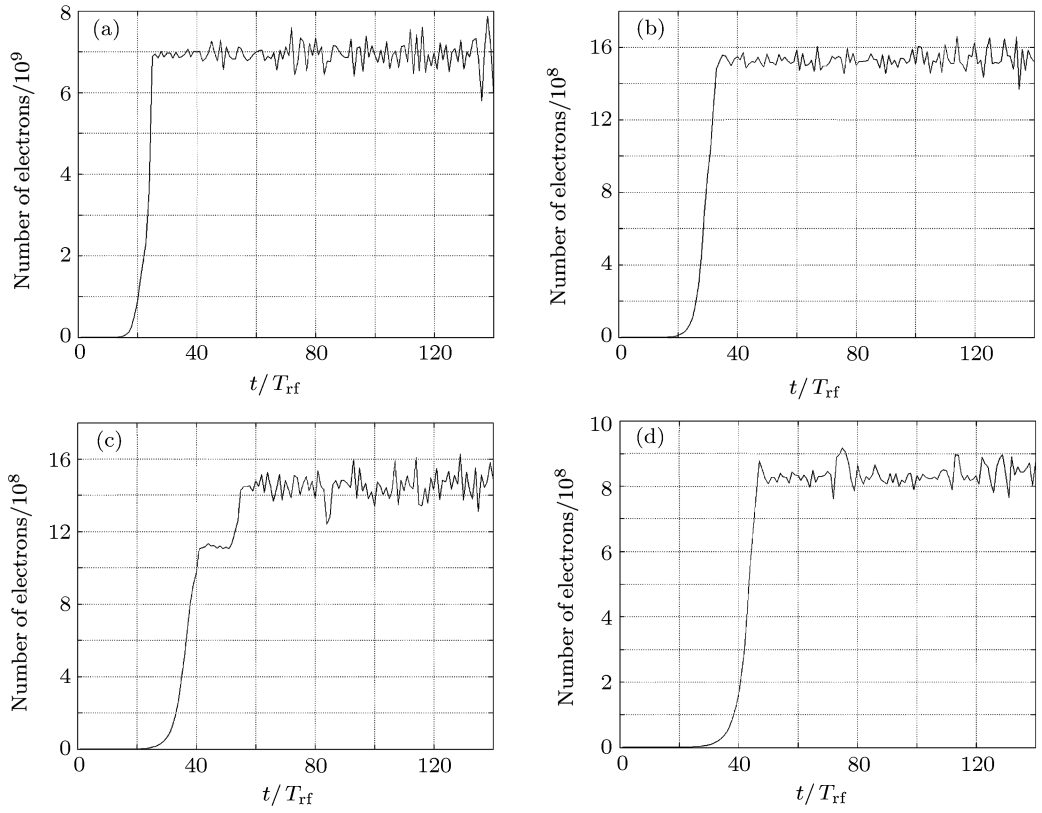


Fig. 7. The temporal evolution of electrons number for different $\alpha_{\rm i}$ for (a) $\alpha_{\rm i} = 5\pi/12$, (b) $\alpha_{\rm i} = \pi/4$, (c) $\alpha_{\rm i} = \pi/6$, and (d) $\alpha_{\rm i} = \pi/12$.

4.2. Effect of the electron oblique incidences on the multipactor susceptibility diagram

The multipactor susceptibility diagrams and time-dependent curves for different electron incidence angles are plotted in Figs. 6 and 7, respectively, where the simulation parameters are taken to be $k = 0.382$, $f = 2 \times 10^9$ Hz, $\delta_{\rm m} = 2.0$, $E_{\rm m} = 400$ eV, and $E_{\rm rf_0} = 1.0$ MV/m.

Figures 4(c) and 6 show that the susceptibility region (where $\delta > 1$) shrinks gradually as the incidence angle $\alpha_{\rm i}$ decreases. Therefore, when the electron incidence angle becomes larger, the multipactor discharge can occur easily and the extremum of δ in the resonant region will be higher.

Figure 7 shows that i) it takes more time for multipactor to reach saturation when $\alpha_{\rm i}$ approaches normal. Therefore, the probability of multipactor discharge decreases when the electron incidence angle approaches normal incidence. As a result, more time is required to reach saturation. ii) When the electron is close to grazing incidence (the larger incidence angle $\alpha_{\rm i}$), the number of electrons in saturation increases, which means that multipactor discharge becomes more serious.

5. Conclusions

The effect of the insulated magnetic field on multipactor susceptibility and the resonant region depends on the initial state of the electrons. The regions expand as the initial phase increases and shrink as initial phase decreases. 1) When the initial phase of electrons is distributed equally, the multipactor susceptibility and the resonant region shift and shrink as the insulated magnetic field increases. The shift and shrinkage are not remarkable when the insulated magnetic field is weak, but they become more evident when the magnetic field is strong enough. 2) When the insulated magnetic field is present, as the electron incidence angle gradually approaches normal, the multipactor occurrence becomes more difficult. The susceptibility region also shrinks gradually and the multipactor saturation level declines gradually.

In practice, according to the demands of device design, electron cyclotron frequency in the insulated magnetic field should be set apart from RF frequency in order to reduce its effects on the multipactor. In this situation, a multipactor can be reduced or restrained effectively by considering RF parameters and the electron incidence angle only. However, when cyclotron frequency is approaches the RF frequency, we recommend that measurements of the magnetic field effect should be taken.

Acknowledgement

The authors gratefully acknowledge Prof. Ding Wu (Institute of Applied Physics and Computational Mathematics) for discussions and recommendations on single-surface multipactor modeling.

References

[1] Robert J Barker and Edl Schamiloglu 2005 *High-Power Microwave Sources and Technologies* (Beijing: Tsinghua University Press) pp. 75, 330 (in Chinese)

[2] Wu L and Anga L K 2007 *Phys. Plasmas* **14** 013105

[3] Sazontov A, Semenov V, Buyanova M and Vdovicheva N, Anderson D, Lisak M, Puech J and Lapierre L 2005 *Phys. Plasmas* **12** 093501

[4] Kim H C and Verboncoeur J P 2006 *Phys. Plasmas* **13** 123506

[5] Cheng G X, Liu L, Liu Y G and Cheng W Y 2009 *IEEE Trans. Plasma Sci.* **37** 1968

[6] Agee Forrest J 1998 *IEEE Trans. Plasma Sci.* **26** 235

[7] Ying X H and Hao J H 2009 *Acta Phys. Sin.* **58** 4799 (in Chinese)

[8] Hao J H, Ding W and Dong Z W 2006 *Acta Phys. Sin.* **55** 4789 (in Chinese)

[9] Vaughan J R M 1993 *IEEE Trans. Electron. Dev.* **40** 83

[10] Vaughan J R M 1988 *IEEE Trans. Electron. Dev.* **35** 1172

[11] Gopinath V P, Verboncoeur J P and Birdsall C K 1998 *Phys. Plasmas* **5** 1535